

## An analytical consideration on aftershock-induced expansion of liquefaction damage of sandy ground with groundwater-level rise due to main shock

Toshihiro Noda<sup>1</sup> and Takahiro Yoshikawa<sup>2</sup>

<sup>1</sup> Disaster Mitigation Research Center, Nagoya University, Furo-cho, Chikusa-ku, Nagoya, Aichi, 464-8603, Japan.

<sup>2</sup> Department of Civil Engineering, Nagoya University, Furo-cho, Chikusa-ku, Nagoya, Aichi, 464-8603, Japan.

### ABSTRACT

Extensive liquefaction damage was observed in the 2011 off the Pacific coast of Tohoku Earthquake over a wide range of reclaimed coastal land. It is reported that in Chiba Prefecture, the large aftershock that occurred 29 minutes after the main shock extended the liquefaction damage in sandy ground. In this paper, using a soil-water-air coupled finite deformation analysis code incorporating the elasto-plastic constitutive equation SYS Cam-clay model, it is shown that the groundwater level rises due to the main shock and that during the aftershock, this groundwater level rise could cause extended liquefaction damage. A special point of emphasis made in this paper is that the results described here could not have been obtained without using the soil-water-air coupled elasto-plastic finite deformation analysis. This is because 1) the generation of positive excess pore water pressure is attributed to the soil contractancy which is described by its elasto-plasticity; 2) determination of behavior of unsaturated soil needs to be based on a three phase system analysis; and 3) settlement/displacement of the ground needs to be calculated precisely by sequential computation in a finite deformation regime.

**Keywords:** soil-water-air coupled analysis; liquefaction; aftershock

### 1 INTRODUCTION

Widespread liquefaction damage was observed in reclaimed coastal land along Tokyo Bay during the 2011 off the Pacific coast of Tohoku Earthquake. The damage was particularly severe in Urayasu City, Chiba Prefecture, despite the fact that the peak ground acceleration observed, around only 200 gal, was not very large. The severe damage has been attributed to the effects of the long duration of the earthquake and the aftershock that occurred 29 minutes after the main shock. Residents of the area have testified that the water which had been oozing out from the ground due to the main shock was intensified by the aftershock (Yasuda et al. 2012). Studies on liquefaction during aftershocks have been carried out exclusively from the standpoint of a soil-water two phase system. For example, Nakai et al. (2013) showed through analysis that the extended liquefaction damage could be attributed to the fact that excess pore water pressure which had increased during the main shock did not dissipate before occurrence of the aftershock. In another study, Morikawa et al. (2013) pointed out the effect of stress-induced anisotropy development that occurred during the main shock.

This paper describes the results of a study performed from the standpoint of a soil-water-air three phase coupled analysis to determine the mechanism of

the extended liquefaction damage caused by aftershocks. By simulating the series of events from a main shock to an aftershock using the soil-water-air coupled finite deformation analysis code (Noda and Yoshikawa, 2015), it is demonstrated that shallow unsaturated sandy ground becomes saturated by the rise in ground water level caused by the main shock and that the aftershock results in the occurrence of liquefaction in this saturated area. This analysis code is an extension of the soil-water coupled finite deformation analysis code (Noda et al., 2008) incorporating the elasto-plastic constitutive equation SYS Cam-clay model (Asaoka et al., 2002), which allows description of the mechanical behavior of a wide range of soils within a single theoretical framework, and is capable of handling soil behavior from deformation to failure regardless of the type of external forces (static/dynamic).

### 2 ANALYTICAL CONDITIONS

The finite element mesh used for analysis is shown in Fig. 1. On the premise that multidimensional flows do not occur, one-dimensional analysis was carried out in this study so that the flow balances of water and air could be determined easily. Computation was performed with respect to the single transverse element mesh, assuming periodic boundary conditions in the

lateral direction and viscous boundary conditions (Lysmer and Kuhlemeyer, 1969) at the bottom face. Assuming a ground depth of 20 m, the initial ground water level was set at 2 m below the ground surface. The initial pore water pressure at the groundwater level was made to coincide with the pore air pressure, and vertically from there, a hydrostatic pressure distribution was assumed. At locations deeper than the ground water level, the initial pore air pressure is equal to the pore water pressure since suction is zero. The pore air pressure was set to zero at the initial ground surface and the pore air pressure at locations shallower than the ground water level was distributed in the vertical direction based on the self-weight of air. The distribution of the initial degree of saturation at locations deeper than the ground water level was calculated according to the hydraulic pressure with consideration to the compressibilities of air and water, assuming that the maximum degree of saturation was at the groundwater level. The distribution at locations shallower than the ground water level was calculated according to the values for suction using the soil water characteristic curve. The hydraulic/air boundary conditions assumed at the ground surface were constant total head condition corresponding to the initial groundwater level and exhausted condition (i.e., always at atmospheric pressure), respectively. All other boundaries were assumed to be in undrained and unexhausted conditions. The soil material was assumed to be uniform across the entire region analyzed, and the material constants and initial values related to the elasto-plastic constitutive equation SYS Cam-clay model were those that had been obtained from mechanical experiments performed on soil samples from the alluvial sand ground in Urayasu City (Nakai et al., 2015). Since the filling soil and alluvial sand layers of the ground in Urayasu contained a high content of fine fractions, the material constants related to the unsaturated seepage characteristics were determined by reference to the existing experimental results for clayey sand (Yamamoto et al., 2009). The material constants and initial values related to the SYS Cam-clay model and the unsaturated seepage characteristics are listed in Tables 1 and 2, respectively. Figure 2 illustrates the soil water characteristic curve of this soil. The input seismic wave is illustrated in Fig. 3. The seismic wave recorded at the K-net Urayasu observation point (CHB008EW) during the 2011 off the Pacific coast of Tohoku Earthquake was modified by “SHAKE” using a model of the ground in the vicinity of the observation point to enable application to the bottom boundaries of the filling soil and alluvial sand layers. A half-wave of the modified seismic waveform was imposed at the bottom boundary in the horizontal direction. For simplicity, the same wave was used as the aftershock and was input 30 minutes after the main shock.

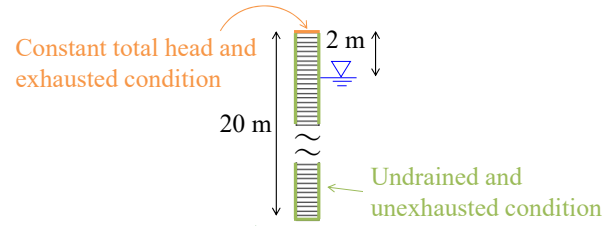


Fig. 1. Finite element mesh.

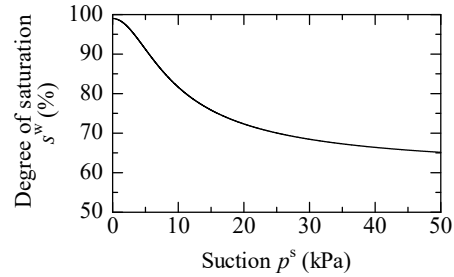


Fig. 2. Soil water characteristic curve.

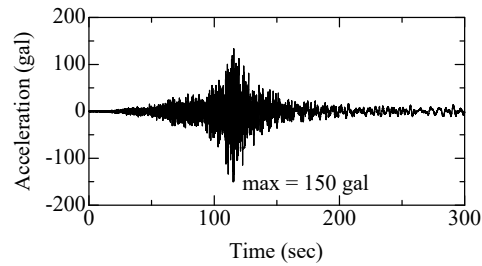


Fig. 3. Input seismic wave.

Table 1. Material constants and initial values related to the elasto-plastic constitutive equation, SYS Cam-clay model.

Elasto-plastic parameters		
Specific volume at $q = 0$ and $p' = 98.1$ kPa on NCL	N	2.0
Critical state constant	M	1.4
Compression index	$\tilde{\lambda}$	0.1
Swelling index	$\tilde{\kappa}$	0.0025
Poisson's ratio	$\nu$	0.1
Evolution rule parameters		
Degradation index of overconsolidation	$m$	8.0
Degradation index of structure	$a$	8.0
Degradation index of structure	$b$	1.0
Degradation index of structure	$c$	1.0
Degradation index of structure	$c_s$	1.0
Evolution index of rotational hardening	$b_r$	10.0
Limit of rotational hardening	$m_b$	0.44
Initial values		
Degree of structure	$1/R_0^*$	3.04
Overconsolidation ratio	$1/R_0$	Distributed
Void ratio	$e_0$	0.98
Stress ratio	$\eta_0$	0.545
Degree of anisotropy	$\zeta_0$	0.0

Table 2. Material constants and initial values related to unsaturated seepage characteristic.

Soil water characteristic		
Maximum degree of saturation %	$s_{max}^w$	99.0
Minimum degree of saturation %	$s_{min}^w$	60.0
van Genuchten parameter $kPa^{-1}$	$\alpha$	0.15
van Genuchten parameter ( $m' = 1 - 1/n'$ )	$n'$	2.0
Saturated coefficient of water permeability m/s	$k_s^w$	$5.0 \times 10^{-4}$
Dry coefficient of air permeability m/s	$k_d^a$	$2.76 \times 10^{-2}$
Physical property		
Soil particle density $g/cm^3$	$\rho^s$	2.787
Bulk modulus of water kPa	$K_w$	$2.19 \times 10^6$
Specific gas constant of air $m^2/s^2/K$	$\bar{R}$	287.04
Absolute temperature K	$\Theta$	293.15

### 3 ANALYSIS RESULT 1: SATURATION OF AN UNSATURATED SURFACE LAYER DUE TO THE MAIN SHOCK

Figure 4 depicts the distributions of the degree of saturation and mean skeleton stress immediately before the main shock, and Fig. 5 depicts those immediately after the main shock. The contour figures are magnified to show the section of the ground up to about 2.5 m from its surface, including the part in which the initial groundwater level was located. It can be seen by comparing the distributions of the degree of saturation immediately before and immediately after the main shock that the ground water level rose during the main shock. With the rise of ground water level, the mean skeleton stress can be seen to decrease in the soil elements with high degrees of saturation. On the other hand, the mean skeleton stress remains relatively high without decreasing much in the soil elements with low degrees of saturation near the ground surface. Figure 6 shows the distribution of the water content variation immediately after the main shock. Due to drainage (plastic volume compression) in the part below the groundwater level, water absorption takes place near the ground surface, and the water content there increases. In other words, the water level rose. In this analysis, pore water movement occurred even during the earthquake because the duration of the earthquake is long and the coefficient of permeability is high.

Figure 7 is a conceptual diagram showing the mechanism that causes the rise in groundwater level. First, consider one-dimensional consolidation of the saturated ground depicted in Fig. 7(a) under drained upper boundary and undrained lower boundary conditions. Since the amount of ground settlement = the amount of water drained from the ground, the level of

the supernatant water produced by drainage during consolidation is equal to the ground surface height before consolidation if we neglect the changes due to evaporation, rainfall, etc. In the current analysis, the part of the ground at or below the initial groundwater level is nearly saturated (degree of saturation = 99% or higher). This part undergoes cyclic shearing during earthquakes under conditions in which sufficient movement of water is not possible (undrained conditions). Therefore, positive excess pore water pressure is generated due to negative dilatancy. As a result, consolidation settlement occurs through dissipation of excess water pressure. However, as shown in Fig. 7(b), when there is unsaturated soil above that part, the water discharged by consolidation is supplied to the unsaturated soil. At this stage, because unsaturated soil is composed of soil particles, pore water, and pore air, the water level rise by the volume of soil (soil particles + pore water + trapped air) that has sunk in the portion corresponding to the supernatant water.

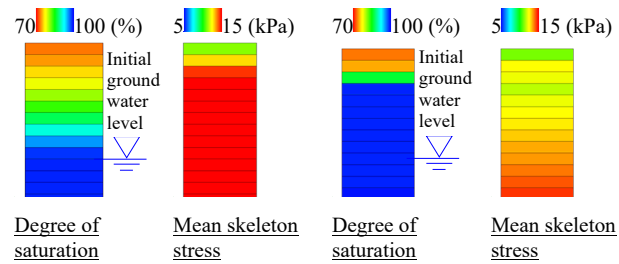


Fig. 4. Distribution of degree of saturation and mean skeleton stress immediately before main shock.

Fig. 5. Distribution of degree of saturation and mean skeleton stress immediately after main shock.

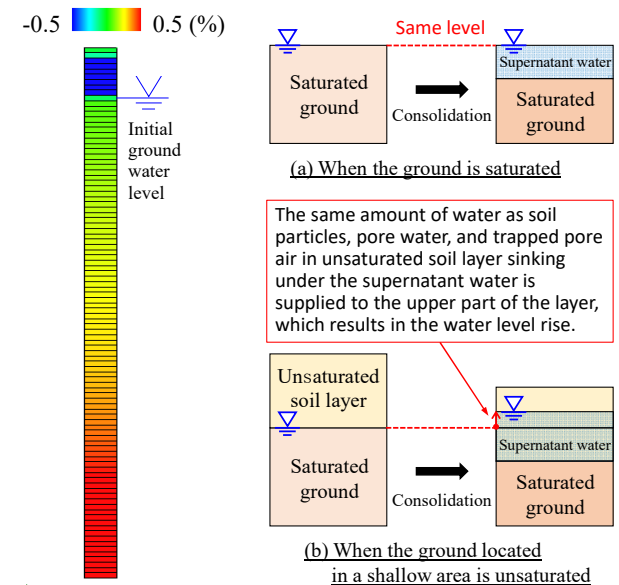


Fig. 6. Distribution of water content variation immediately after main shock.

Fig. 7. Mechanism of groundwater level rise.

#### 4 ANALYSIS RESULT 2: EXTENSION OF THE LIQUEFIED AREA DUE TO THE AFTERSHOCK

Figure 8 depicts the distributions of the degree of saturation and mean skeleton stress immediately before the aftershock, and Fig. 9 depicts those immediately after the aftershock. Just before the aftershock, although the mean skeleton stress recovered due to the dissipation of excess pore water pressure, the degree of saturation near the ground surface rose further. Since the aftershock occurred in a state where the degree of saturation was high near the ground surface, the mean skeleton stress immediately after the aftershock decreased to a level lower than that after the main shock. In addition, the groundwater level rose further due to the aftershock and reached the ground surface. This behavior is consistent with the report of Yasuda et al. (2012) cited in INTRODUCTION. In other words, one of the factors that cause extended liquefaction during aftershocks is the saturation of the unsaturated area near the ground surface due to a rise in groundwater level during and after the main shock. Although figures or data are not shown in this paper due to limitations in terms of available space, the risen water level was observed to have returned eventually to the level before the earthquake (initial groundwater level) because of the pre-set analytical condition of a constant water head on the ground surface.

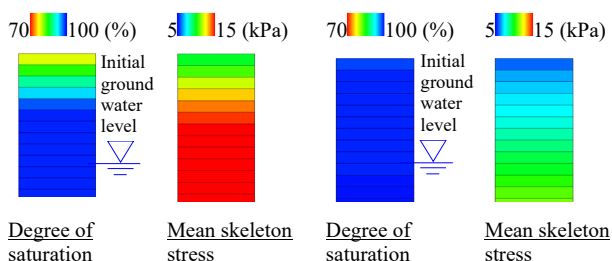


Fig. 8. Distribution of degree of saturation and mean skeleton stress immediately before aftershock.

Fig. 9. Distribution of degree of saturation and mean skeleton stress immediately after aftershock.

#### 5 CONCLUSION

The mechanism of extended liquefaction occurrence during aftershocks was investigated by simulating the series of processes from a main shock to an aftershock using a soil-water-air coupled elasto-plastic finite deformation analysis code. This study identified the following mechanisms. 1) Because of the external seismic forces, the saturated part of the soil at and below the ground water level is subjected to cyclic shear while it is in a state where drainage cannot take place immediately. As a result, excess pore water pressure is generated due to negative dilatancy. 2) If the duration of the earthquake is long, consolidation drainage (plastic volume compression) occurs not only

after but also during the earthquake. As a result, pore water is supplied from the saturated soil to the unsaturated soil above the ground water level. 3) The ground water level rises, and the saturated area expands between the main shock and after shock. Since the ground is subjected to the aftershock in such a state, the sand layer that is liquefied becomes larger, resulting in extended liquefaction damage.

The phenomenon of groundwater level rise during an earthquake, which occurs as a result of plastic volume compression of the soil, cannot be described by an analysis that assumes soil to be an elastic body. Furthermore, it is necessary to determine the amount of settlement precisely through sequential computation. Therefore, it needs to be emphasized that the analytical results described in this paper could not have been obtained without using the soil-water-air three phase coupled elasto-plastic finite deformation analysis.

#### ACKNOWLEDGEMENTS

This work was supported by JSPS KAKENHI Grant Numbers 25249064 and 17H01289.

#### REFERENCES

- Asaoka, A., Noda, T., Yamada, E., Kaneda, K. and Nakano, M. (2002). An elasto-plastic description of two distinct volume change mechanisms of soils. *Soils and Foundations*, 42(5), 47-57.
- Lysmer, J. and Kuhlemeyer, R.L. (1969). Finite dynamic model for infinite media. *ASCE*, 95(EM4), 859-877.
- Morikawa, Y., Bao, X., Zhang, F., Taira, A. and Sakaguchi, H. (2013). Why an aftershock with a maximum acceleration of 25 gal could make ground liquefied in the 2011 Great East Japan Earthquake. *Proc. of 6th International Workshop on New Frontiers in Computational Geotechnics*, 117-122.
- Nakai, K., Noda, T. and Asaoka, A. (2013). Main shock-aftershock interval effect on the liquefaction damage in Tohoku Region Pacific Coast Earthquake. *Japan Geoscience Union Meeting 2013*, SSS33-P24.
- Nakai, K., Asaoka, A. and Sawada, Y. (2015). Liquefaction damage enhanced by interference between the body wave and surface wave induced from the inclined bedrock. *Japanese Geotechnical Society Special Publication*, 2(19), 723-728.
- Noda, T., Asaoka, A. and Nakano, M. (2008). Soil-water coupled finite deformation analysis based on a rate-type equation of motion incorporating the SYS Cam-clay model. *Soils and Foundations*, 48(6), 771-790.
- Noda, T. and Yoshikawa, T. (2015). Soil-water-air coupled finite deformation analysis based on a rate-type equation of motion incorporating the SYS Cam-clay model. *Soils and Foundations*, 55(1), 45-62.
- Yasuda, S., Harada, K. and Ishikawa, K. (2012). Damage to structures in Chiba Prefecture during the 2011 Tohoku-Pacific Ocean Earthquake. *Japanese Geotechnical Journal*, 7(1), 103-115 (in Japanese).
- Yamamoto, T., Nakai, T., Maruki, Y., Kodaka, T., Kishida, K. and Ohnishi, Y. (2009). Health assessment of the slopes along the roads introducing the long-term degradation concept. *Japanese Geotechnical Journal*, 4(1), 21-33 (in Japanese).